NATIONAL AERONAUTICS AND SPACE ADMINISTRATION

Technical Memorandum 33-458

Microwave Emission From Granular Silicates: Determination of the Absorption Coefficient From Plate Measurements and the Effects of Scattering

J. E. Conel

JET PROPULSION LABORATORY
CALIFORNIA INSTITUTE OF TECHNOLOGY
PASADENA, CALIFORNIA

October 15, 1970

NATIONAL AERONAUTICS AND SPACE ADMINISTRATION

Technical Memorandum 33-458

Microwave Emission From Granular Silicates: Determination of the Absorption Coefficient From Plate Measurements and the Effects of Scattering

J. E. Conel

JET PROPULSION LABORATORY
CALIFORNIA INSTITUTE OF TECHNOLOGY
PASADENA, CALIFORNIA

October 15, 1970

Prepared Under Contract No. NAS 7-100
National Aeronautics and Space Administration

Preface

The work described in this report was performed by the Space Sciences Division of the Jet Propulsion Laboratory.

Acknowledgment

The field experiments discussed in this report were designed and carried out by John Blinn and associates, Jet Propulsion Laboratory, and by Jack Quade and his team, University of Nevada. A. A. Loomis and G. B. Holstrom participated in the field operations and in subsequent discussions. The support of all these individuals is gratefully acknowledged. The author has also benefited greatly from discussions with R. J. Phillips. Both he and D. B. Nash supplied helpful criticisms of this work. The assistance of Elsa Abbott and Patricia B. Conklin is also acknowledged.

Contents

Tables

Figures

Abstract

Microwave brightness temperature measurements (1.4–37 GHz) from plane layers of granulated silicate materials backed by a perfectly reflecting metal plate are used to determine the mass absorption coefficient, attenuation length, and effective values of electrical conductivity and loss tangent. The important experimental finding is that the mass absorption coefficient is independent of frequency but highly dependent on moisture content. From this one determines that the effective conductivity increases with frequency, and that the loss tangent is independent of frequency in this frequency range. Computed values of these quantities are in rough numerical agreement with extrapolated laboratory values on other silicate materials. The effects of scattering, using elementary solutions of the equation of radiative transfer, are described.

Microwave Emission From Granular Silicates: Determination of the Absorption Coefficient From Plate Measurements and the Effects of Scattering

I. Introduction

This report describes a simple theory and experiment for determining microwave mass absorption coefficient in a loose granular medium. The results of a program of actual field measurements are reported and compared with the theory. The field operations themselves, the measurement techniques, and the method of data reduction are described in Refs. 1–3.

Planetary passive microwave observations are usually described in terms of a theory given by Piddington and Minnett (Ref. 4), in which the emitting homogeneous medium is taken to be in local thermodynamic equilibrium and radiating in the microwave region according to the Rayleigh–Jeans law. The temperature distribution with depth is determined from the theory of heat conduction with the condition of known temperature at the surface. The effective microwave brightness temperature is obtained by integrating the equation of radiative transfer to obtain an expression for the emergent intensity.

On the basis of this theory, the most one can hope to learn about planetary surfaces from passive microwave measurements is the average absorption and scattering properties of the near-surface materials and gross estimates of electrical properties, together with the near-surface temperature distribution (in nonscattering media) and thermal properties. From these data, one may indirectly draw inferences about the physical state of aggregation and the surface atmospheric pressure. It may, in principle, be possible to detect nonhomogeneities in surface properties in an isothermal medium provided they are of simple geometry (plane-parallel stratification), and providing the absorption and scattering coefficients increase essentially discontinuously with depth.

Rough determinations of surface rock type may be possible, but this conclusion rests, of course, on the largely unknown dependence of microwave properties on rock composition *and* state of physical aggregation, and on low abundance or absence of adsorbed or pore water. An extremely optimistic use of combined surface infrared and subsurface microwave temperature data is determination of planetary heat flow. Such an analysis has been attempted by Baldwin (Ref. 5) for the moon. A recent summary of microwave observations of the moon is given in Ref. 6.

Perturbations introduced by the atmosphere have been neglected because the path lengths for all observations reported here are short. These effects can be discussed in the light of known effects on microwave propagation through the atmosphere of the earth or in field operations accounted for by methods similar to those described here. Contributions of reflected sky background radiation to the observed intensity have also been neglected.

Buried plate experiments, in which actual geological materials are used, offer a simple means of verifying the theory outlined and provide a method (under certain restrictions) of deriving useful approximate information on electrical properties of rocks in the microwave region. In an idealized plate experiment, a plane layer of homogeneous material of thickness l and at constant temperature is superimposed above an (assumed) perfectly reflecting metal plate. The intensity of microwave energy emergent from the upper surface is measured. From a series of such measurements made with layers of different thickness, an effective microwave absorption coefficient of the material may be obtained directly.

II. Theory of Radiative Transfer Applied to Plate Problems

To describe this experiment qualitatively in terms of the theory of radiative transfer, the medium is assumed to be absorbing and the scattering is assumed to be zero. For actual silicates, this assumption is never rigorously true, but the assumption permits simplification of the analysis. Approximate conditions of nonscattering can be realized where particles of complex refractive index $\mathbf{n} = n + in'$ are immersed in a medium of real refractive index n, with n' very small, or in situations of independent scattering where particle radius is small compared to the wavelength. The effects contributed by inclusion of scattering in the theory are discussed later.

Let the mass absorption coefficient of the medium at wavelength λ be $k_\lambda(x)$ and the density $\delta(x)$, where x is a coordinate measured perpendicular to the layer. Then the incremental optical thickness $d\tau$ is given by $k_\lambda(x)\delta(x)\,dx$. For the experimental arrangement shown in Fig. 1, one desires the specific intensity of radiation in direction θ at wavelength λ emergent from a layer of normal optical thickness τ_1 given by

$$\tau_1 = \int_0^l k_\lambda(x)\delta(x)\,dx$$

At $\tau = 0$, the intensity is composed of three parts:

(1) The beam emitted in direction θ composed of contributions from incremental layers along this direction, each contribution being attenuated by intervening material.

(2) The beam emitted in a direction $\pi - \theta$ that is specularly reflected at τ_1, and emerges in direction θ after attenuation by the layer.

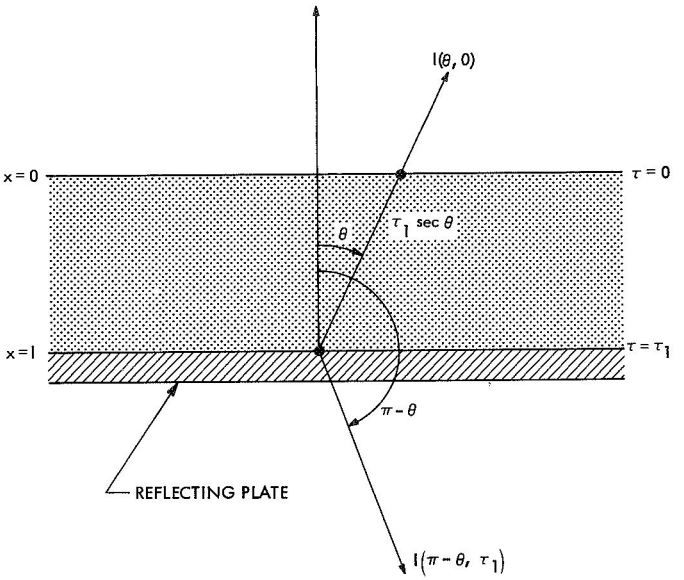

Fig. 1. Geometry of the plate experiment

(3) Energy emitted in direction θ by the reflecting plate and attenuated in the layer.

The specific intensity $I_\lambda(\tau, \theta)$ at $\tau = 0$ in direction θ is

$$I_\lambda(0, \theta) = \int_0^{\tau_1} B_\lambda(t) e^{-t \sec\theta} \sec\theta\, dt \qquad (1)$$

where $B_\lambda(t)$ is the Planck function, approximated in the microwave region by the Rayleigh–Jeans law

$$B_\lambda(T) = \frac{AT}{\lambda^4}$$

where A is a constant and T is absolute temperature. In Eq. (1), if one lets $\tau_1 \to \infty$, the law of darkening $I_\lambda(0, \theta)$ obtained is the Laplace transform of the source function $B(t)$ with $\sec\theta$ the transform variable. Thus, in a nonscattering semi-infinite homogeneous medium, measurement of $I_\lambda(0,\theta)$ offers the possibility of determining temperature distribution with depth. The inversion problem would be analogous to that of temperature sounding in a homogeneous, constant-pressure atmosphere using radiation measurements in gas absorption bands (see Ref. 7 for the problem in a real atmosphere). The fact that silicates scatter as well as absorb radiation at most frequencies, however, prevents determination of actual physical temperature by these methods. If B is constant (i.e., T is not a function of position),

$$I_\lambda(0,\theta) = B_\lambda(T)\,(1 - e^{-\tau_1 \sec\theta}) \tag{1a}$$

In general, however, one can see from Eq. (1) that the emergent intensity is a function both of temperature distribution and the spatial variation of material properties. In the general case, inversion of this expression to obtain either distribution would not be unique. In subsequent equations, for convenience, the subscript and notation indicating angular dependence will be dropped with the understanding that the appropriate quantities are functions of both wavelength and angle. The media are assumed to be homogeneous and at constant temperature. The total intensity in direction θ emergent at $\tau = 0$ is, therefore,

$$I(0)_{\tau_1} = B(T)[1 - e^{-\tau_1 \sec\theta} + \rho e^{-\tau_1 \sec\theta}\,(1 - e^{-\tau_1 \sec\theta})] + (1 - \rho)\,B(T_p)e^{-\tau_1 \sec\theta} \tag{2}$$

where ρ is the reflectance of the plate and T_p is its absolute temperature, which in thermal equilibrium will equal T. The subscript τ_1 means that the intensity is computed for a layer of normal optical thickness τ_1. It shall be assumed hereafter that $\rho = 1$, in which case Eq. (2) reduces to

$$I(0)_{\tau_1} = B(T)\,(1 - e^{-2\tau_1 \sec\theta}) \tag{3}$$

From Eq. (3) $I(0)_{\tau_1} \to B(T)$ as $\tau_1 \to \infty$, so that the ratio of the intensity emergent from a layer of optical thickness $\tau_1 \sec\theta$ to that from an infinitely thick medium, both at constant temperature T, provides a value of τ_1 and, hence, k if δ and l are measured independently. Thus,

$$\frac{I(0)_{\tau_1}}{I(0)_\infty} = 1 - e^{-2\tau_1 \sec\theta} \tag{4}$$

This expression is independent of temperature if the experiment is carried out isothermally. In practice, this condition may be difficult to maintain for several reasons, among which are the following:

(1) Field observations are time consuming; changes in solar insolation because of changes in cloud cover or diurnal passage of the sun may alter material temperatures substantially during an experiment.

(2) Large quantities of material are required to fill adequately the radiometer field of view, and proper burial of the plate usually requires taking material initially beneath the surface, which may be at a different temperature and have a variable moisture content as well.

Nonisothermal conditions can be accounted for with an increase in mathematical complexity (see Appendix). Studies of nonisothermal effects will be the object of future experimental work.

Materials at the surface of the earth are often nonhomogeneous with depth, either as a result of weathering (i.e., most soils show characteristic "profiles" composed of two or more distinct layers or soil horizons) or perhaps because of depositional processes involved. These features are illustrated in Fig. 2, which shows a poorly developed soil horizon (root structures of *Lupinus spp.* emerging from lower part) overlying crudely stratified pumiceous gravel (Mono Craters). For plate measurements reported here, these materials were "homogenized."

It should be noted that from Eq. (4), one could determine $k\delta$ from measurements at two angles θ, for one layer thickness l, if the angular dependence of the actual surface emissivity were known. For homogeneous media, angular measurements thus offer the possibility of remote determination of near-surface microwave properties as well as temperature distribution with depth in a nonisothermal semi-infinite medium. In this case, as has been noted, the temperature distribution is obtained in principle by inverting the Laplace transform of $B(t)$, as shown in Eq. (1).

Fig. 2. Stratification in pumiceous gravel at Mono Craters

III. Discussion of Experiments

A series of microwave radiometer measurements (at wavelengths of 0.8, 2.2, 3.2, and 21 cm) was carried out at three sites: Mono Craters, Calif., Reno, Nev., and Poison Lake, near Mt. Lassen, Calif. The technical details of this program are reported elsewhere (Refs. 1 and 2); herein examples of the data obtained are given and the theory outlined earlier is applied to the data.

Figure 3 shows the physical arrangement of radiometer and metal reflecting surface at the Poison Lake site. In all of the experiments, the reflecting surface (consisting of an arrangement of 1.5×1.5 m aluminum plate and aluminum foil) was buried at various depths in sand, gravel, or cinders of roughly uniform particle size. Near-normal incidence ($\theta \leq 15$ deg) brightness temperatures were measured as a function of particle size, moisture content, and wavelength. Layer thickness was measured in several places over the observed area to the nearest centimeter, and a special attempt was made to keep the layer boundaries plane-parallel. Nevertheless, the true average thickness of a layer is uncertain, perhaps by 2 or 3 cm in thicker layers. Such errors are, of course, especially important in measurements on thin layers. The estimated value of $I(0)_\infty$ was obtained by increasing layer thickness until changes in observed brightness temperature were within experimental error limits.

Fig. 3. Poison Lake cinder pit radiometer site

To illustrate the results, data at various wavelengths are given in Fig. 4 for a test in pumiceous beach sand (Mono Lake) with constant grain size and moisture content. The parameter $\psi(l) = 1 - I(0)_l/I(0)_\infty$ is plotted as a function of layer thickness, where $I(0)_l$ means intensity emergent from a layer of actual thickness l. Where present, horizontal bars on the ordinate parameter at each value of l represent differences in $\psi(l)$ arising from differences in brightness temperature obtained for the radiometer antenna set to measure horizontally or vertically polarized radiation. Straight lines have been fitted to the data by eye. A generally linear relationship between the ordinate parameter and layer thickness is indicated, as predicted by Eq. (4). The slope of any line is then proportional to $-2k\delta$. The scatter in experimental points may arise from changes in experimental condi-

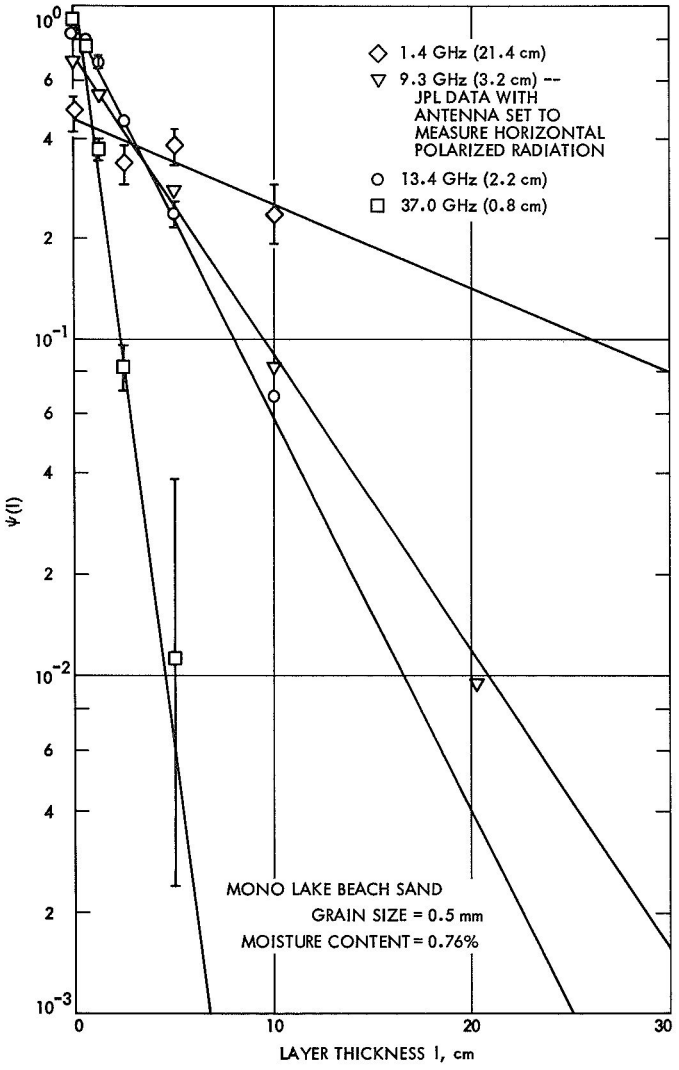

Fig. 4. Parameter $\psi(l)$ as a function of layer thickness

tions during the observations (see Ref. 3) or from uncertainties in average layer thickness. On the other hand, the variations may be real, and thus indicative of defects in the simple theory used here.

Equation (3) shows that $I(0)_{\tau_1} \to 0$ as $\tau_1 \to 0$, corresponding to the physical fact that radiation in absorbing media is emitted only by finite volumes, not "surfaces." In Fig. 2, it should be noted that lines drawn through the data points do not intersect the "origin" $\psi(0) = 1$; the departure increases with increasing wavelength. Among the possible contributors to this discrepancy are:

(1) Systematic uncertainty in measured layer thickness.

(2) Reflectance of metallic substrate, $\rho \neq 1$.

(3) Failure of the theory at longer wavelengths.

(4) Radiometer beamwidth field of view exceeds reflecting plate dimension solid angle of the plate subtended at the antenna.

(5) Experimental error.

(6) Sky background radiation (equivalent temperature near 5°K) reflected by the plate.

Hypothesis (1) may be discarded as a major source of difficulty because the required systematic errors in measurement of layer thickness would necessarily be "wavelength dependent," and at $\lambda = 21$ cm of the order of 150% of the layer thicknesses themselves. The reflectance of aluminum may be affected by the presence of a partially oxidized layer with the oxide acting as a dielectric. For wavelengths considered here (0.8–21 cm), the skin depth in aluminum is on the order of 10^{-4}–10^{-5} cm, and it is easy to imagine oxidation occurring to this depth or greater on the plate surfaces. Thus, from Eq. (2)

$$\lim_{\tau_1 \to 0} I(0)_{\tau_1} \neq 0$$

The possible importance of this effect is experimentally undetermined.

Reflected sky radiation and plate emission are observationally indistinguishable from other forms of background radiation. Sky contributions are ordinarily considered negligible at the longer wavelengths of interest here, where the discrepancy discussed is most pronounced.

One might expect the present theory to break down when particle size is much less than the wavelength considered, and, under such conditions, for some form of continuum theory to apply. Reflection of partially coherent light at layer boundaries would give rise to interference effects that could be expected to manifest themselves among other ways as: (1) periodic variations in brightness temperature at constant wavelength for varying layer thickness, or (2) periodic variations in brightness temperature as a function of wavelength for constant layer thickness. The available experimental data are inadequate for detecting such effects.

The systematic wavelength dependence of the departures of these lines from the origin suggests hypothesis (4) to be the most important contributing effect. Beamwidths of the radiometers involved are known to be wavelength dependent,* the angular width increasing with increasing wavelength. Thus, "background" radiation is collected from surface and terrain adjacent to the plate as well as from the plate region. In future experiments, problems of this sort can be reduced by use of larger reflecting areas.

In Fig. 5, the attenuation length $\alpha = (k\delta)^{-1}$ is plotted as a function of wavelength for Mono Beach sand and basaltic cinders from Poison Lake; α represents the distance in which the intensity of light falls to $1/e$ of its initial value. The general increase of α with frequency is similar to that found for other earth materials, but at lower frequencies (Ref. 8).

To make connections with electromagnetic theory and obtain estimates of electrical properties in the microwave region, we may define an effective complex refractive index for a homogeneous medium with scatterers $\mathbf{n}_e = n_e + in'_e$. The assumptions required for this step, connections with scattering theory, and restrictions on use of the complex index so obtained are outlined by Van de Hulst (Ref. 9). The comparison with scattering theory will apply strictly only if conditions of single scattering obtain (i.e., mutual particle distances are $\gg \lambda$), and if $\mathbf{n}_e \simeq 1$. While these conditions are obviously not satisfied in detail in a condensed particulate medium, results obtained with their use conform qualitatively to those obtained by other methods both in frequency dependence and magnitude.

From electromagnetic theory (Ref. 10, p. 614), the penetration depth d is

$$d = \lambda_0 / 4\pi n'_e$$

*Blinn, J. C., personal communication.

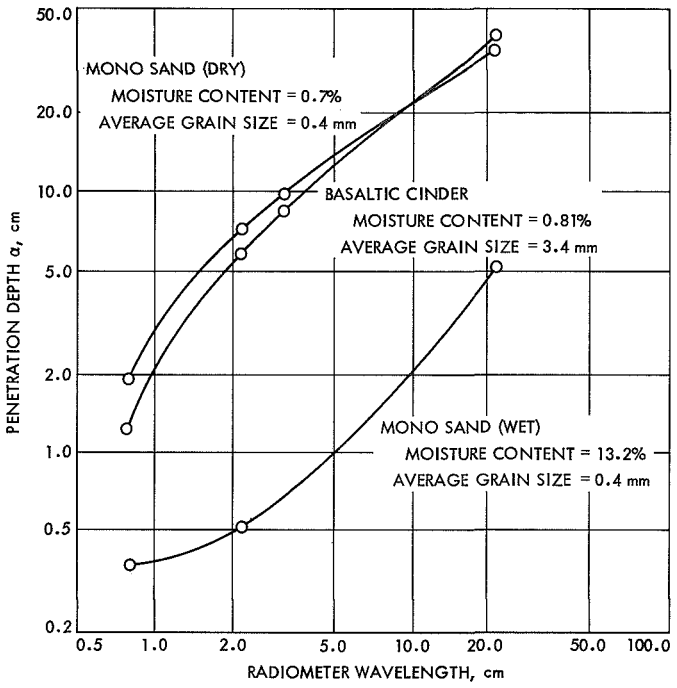

Fig. 5. Penetration depth vs wavelength for sand and cinders

where λ_0 is the wavelength in vacuum and $4\pi n'_e$ is the absorption coefficient. In this case, d represents a length over which the energy density associated with an advancing plane wave is reduced to $1/e$ of its initial value. By equating α and d (under the assumptions stated), one obtains n'_e as a function $k\delta$. The quantity n'_e obtained in this manner is given in Table 1 for the materials studied, both wet and dry.

There are two important features in the data. First, there is no apparent systematic dependence of n'_e on frequency. Second, the value of n'_e is highly dependent on moisture content.

In Fig. 6, values of the effective conductivity σ_e (given in mhos/meter) are plotted as a function of frequency. These have been computed as shown in the following. From Stratton (Ref. 11, p. 324), we define an effective attenuation factor β_e for the medium in terms of n'_e by the equation

$$n'_e = \frac{\beta_e c}{\omega} \tag{5}$$

where c is the velocity of light and ω is frequency (sec^{-1}). The effective attenuation factor is (Ref. 10, p. 276)

$$\beta_e = \omega \left\{ \frac{\mu_0 \epsilon_0 K}{2} \left[\left(1 + \frac{\sigma_e^2}{\epsilon_0^2 K^2 \omega^2} \right)^{1/2} - 1 \right] \right\}^{1/2} \tag{6}$$

in which

K = relative dielectric constant

ϵ_0 = permittivity of free space = 8.854×10^{-12} F/m

μ_0 = permeability of free space = 4×10^{-7} H/m

Using Eq. (5) and solving Eq. (6) for σ_e, one finds

$$\sigma_e = 2\pi \epsilon_0 K f \left\{ \left[1 + \frac{2(n'_e)^2}{\mu_0 \epsilon_0 c^2 K} \right]^2 - 1 \right\}^{1/2} \tag{7}$$

where f is frequency in gigahertz. When numerical values are inserted,

$$\sigma_e = 5.563 \times 10^{-11} K f \left\{ \left[1 + 6.275 \frac{(n'_e)^2}{K} \right]^2 - 1 \right\}^{1/2} \tag{8}$$

No independent measurement of K for any of these materials is available. Under circumstances where $\sigma_e^2/\epsilon_0^2 K^2 \omega^2 \ll 1$, the reflection coefficient for a plane surface (i.e., surface irregularities $\ll \lambda$ in height) is dependent only on the dielectric properties (Ref. 10, p. 510). Hence, an estimate of K could be obtained in this case from angular measurements and determination of the Brewster angle. In general, however, for granular silicate with even low moisture content, this inequality does not apply, and the Brewster angle is a complicated function of both the dielectric constant and the conductivity. In the present instance, one can obtain a likely range of values by extrapolating, in frequency, data on the dielectric constant of wet and dry basalt, volcanic ash, and salty ice given by Ward, et al. (Ref. 12). From these data, $2 < K < 10$ at 10^9 Hz; for the two extremes of σ_e shown in Fig. 6, the low values correspond to the case $K = 2$, and high values to $K = 10$.

High values of the conductivity are correlated with high moisture content, and there is generally an increase in conductivity with increasing frequency in this range of frequencies.

In Fig. 7, values of the effective loss tangent given by $\tan \delta_e = \sigma_e/\epsilon_0 K\omega$ are plotted as functions of frequency. Using Eq. (7), one finds

$$\tan \delta_e \sim 2n'_e / (K)^{1/2} \tag{9}$$

Table 1. Geologic and radiative properties of materials at Mono Craters, Reno, and Poison Lake sites

Geologic properties						Radiative properties			
Site designation and location	Particle size, mm		Weight percent water	Density, g/cm^3	Partial site description	Wavelength λ, cm	Frequency f, GHz	Attenuation length, cm	n_e'
	Mean	Standard deviation							
Mono 1 (dry), Mono Craters	1.43 1.20	2.80 3.70	0.27	1.19	Open pumice flats adjacent to Mono craters. Sparse vegetation, poorly sorted gravel with max fragment 3 cm in diameter. Fines removed from plate samples by wind action	2.2 0.8	13.4 37.0	8.2 1.8	0.02 0.04
Mono 2 (dry), Mono Lake	0.42	0.33	0.67	1.14	Beach, south side of Mono Lake. Fine to coarse, unconsolidated sand composed mostly of pumice, quartz, feldspar, partial cementation with evaporites from lake water	21.0 3.2 2.2 0.8	1.4 9.3 13.4 37.0	34.4 9.7 7.2 1.9	0.05 0.03 0.02 0.03
Mono 2 (wet), Mono Lake	0.46	0.24	13.23	1.14	Sand moist with briny water from Mono Lake	21.0 2.2 0.8	1.4 13.4 37.0	5.1 0.52 0.37	0.34 0.34 0.17
Reno 1 (dry), Reno	12.6	2.53	0.11	1.17	Nevada Aggregate and Gravel Co. pit; pumice aggregate	3.2 2.2 0.8	9.3 13.4 37.0	5.5 2.6 1.1	0.05 0.07 0.06
Reno 2 (dry), Reno	5.40	1.68	0.92	1.50	Gravel pit; angular crushed pumice aggregate	3.2 2.2 0.8	9.3 13.4 37.0	6.8 4.0 3.3	0.04 0.04 0.02
Reno 2 (wet), Reno	5.40	1.68	6.53	1.50	Gravel pit; gravel dampened with Reno municipal water	3.2	9.3	0.65	0.39
Lassen 1 (dry), Poison Lake	3.4	2.5	0.81	1.10	Well sorted basalt cinders, partially oxidized	3.2 21.0 2.2 0.8	9.3 1.4 13.4 37.0	8.6 40.3 5.8 1.25	0.03 0.04 0.03 0.05

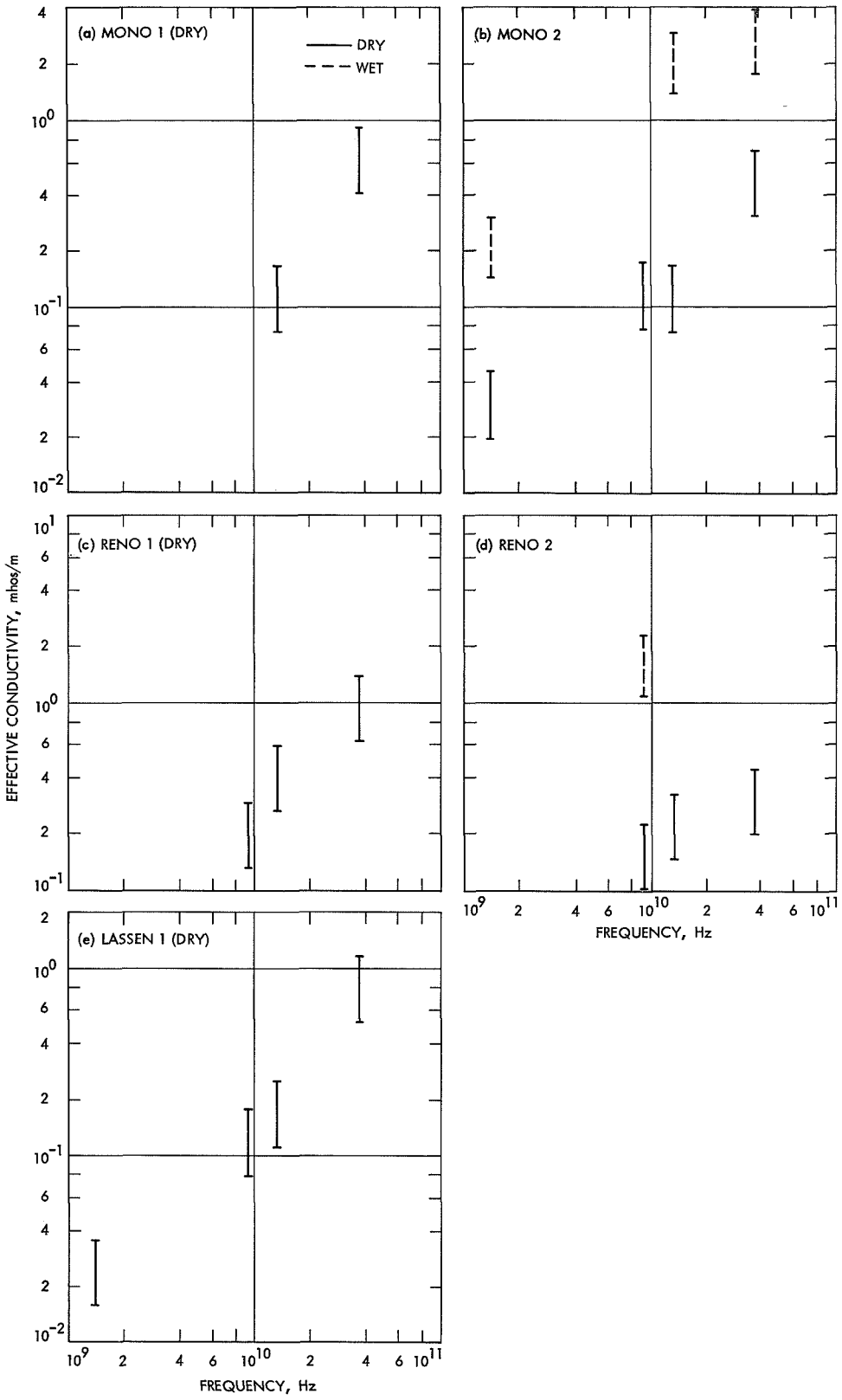

Fig. 6. Calculated conductivities for various wet and dry materials, and the variations with frequency

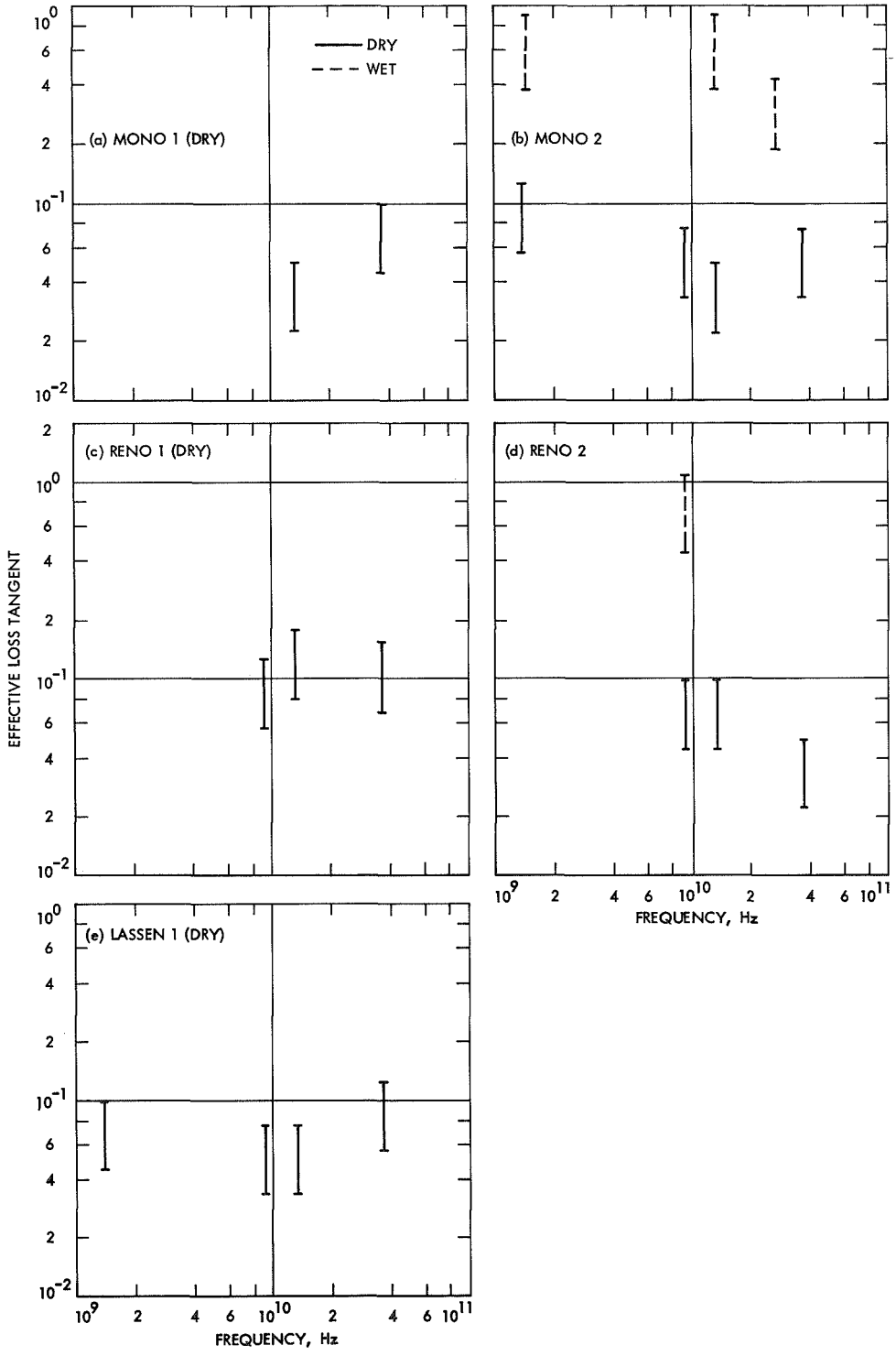

Fig. 7. Effective loss tangents for various wet and dry materials, and the variations with frequency

In terms of the loss tangent, the penetration depth d is $d = \lambda_0/(2\pi K^{1/2} \tan \delta_e)$. As before, the range of values corresponds to $2 < K < 10$. It can be seen from the data that, because of the functional dependence, like n'_e, $\tan \delta_e$ is numerically highly dependent on moisture content and has no obvious dependence on frequency.

In computing conductivities and loss tangents, it has been assumed that the value of $k\delta$ deduced from slopes of lines in Fig. 3 represents the actual value of the absorption coefficient. It has also been noted that, contrary to theory, $\psi(0) \neq 1$, and the difficulty has been attributed principally to background effects. Accepting this as a plausible explanation, one can demonstrate how this effect influences values of σ_e and $\tan \delta_e$ calculated from the theory. For the purpose of illustration, edge effects in the radiometer field of view will be accounted for approximately by neglecting the angular distribution of radiation in the emergent field and angular dependence of the antenna patterns. The observed intensity is taken as

$$I(0)_l = I_p e^{-k\delta l} + I_b e^{-k\delta l} + B(T)\,(1 - e^{-2k\delta l}) \qquad (10)$$

where

I_p = intensity of light emitted by the plate

I_b = intensity of background radiation

The third term on the right-hand side of Eq. (10) represents radiation emitted by a layer of actual thickness l at temperature T over the radiometer field of view. The parameter $\psi(l)$ is

$$\psi(l) = e^{-k\delta l}\left[e^{-k\delta l} - \left(\frac{I_p + I_b}{B(T)}\right)\right] \qquad (11)$$

and

$$\psi(0) = 1 - \frac{I_b + I_p}{B(T)} \qquad (12)$$

The factor $C = 1 - \psi(0)$ is given in Table 2 for the data in Fig. 3.

Table 2. Errors in measured values of $k\rho$ arising from edge effects

Frequency, GHz	C	$[d \ln \Psi(l)/dl]_{l=0}$	Fractional error
1.4	0.54	3.2k	0.2
9.3	0.29	2.4k	0.07
13.4	0.09	2.1k	0.02
37.0	0.00	2.0k	0.0

Differentiating Eq. (11) with respect to l, one finds

$$\frac{d \ln \psi(l)}{dl} = -2k\delta - C\frac{k\delta\, e^{k\delta l}}{1 - C\, e^{k\delta l}} \qquad (13)$$

so that the apparent value of $k\delta$ found by measuring $d \ln \psi/dl$ and solving Eq. (13) would depend on l. At $l = 0$

$$\left.\frac{d \ln \psi(l)}{dl}\right|_{l=0} = -\left(\frac{2 - C}{1 - C}\right)k\delta \qquad (14)$$

The factor $C/2(1 - C)$, given in column 3 of Table 2, represents the fractional errors introduced in determination of n'_e for the value of C indicated from the slope at $l = 0$. The estimated values of n'_e are, in general, too large in this case, the errors decreasing with increasing frequency. From Eqs. (8) and (9), the low-frequency values of σ_e and $\tan \delta_e$ are systematically too large, according to these arguments; from Eq. (4a), the values of d are too small. From Eq. (13), the slope at $l \to \infty$ would give $k\delta$ directly independent of C. In this instance, however, $\psi = 0$. Thus, errors of 50% in values of σ_e, $\tan \delta_e$, and d may be encountered with experimental problems of the type described.

In Figs. 8 and 9, the present data on effective conductivity and loss tangent are compared with those of Ward, et al. (Ref. 12) obtained by conventional laboratory methods for wet and dry basalts, volcanic ash, and salty ice. For such comparisons, it is necessary to extrapolate the laboratory data over a frequency range of three orders of magnitude. Because these extrapolations are untrustworthy and because of the general dissimilarities in rock type and moisture content, one obviously cannot make quantitative comparisons. However, it is worth noting that frequency dependence and order of magnitude of mean values of the computed quantities are roughly in agreement with measured values, although, as has been shown, the computed values are higher than predicted by extrapolation.

Frequency dependence of the effective conductivity and apparent frequency independence of the effective loss tangent follow from Eqs. (8) and (9), together with: (1) the present experimental result that n'_e is essentially independent of frequency, and (2) the assumption (suggested by laboratory data) that K is largely constant in this frequency range.

The agreement secured may appear surprising in view of the gross assumptions required to define an effective

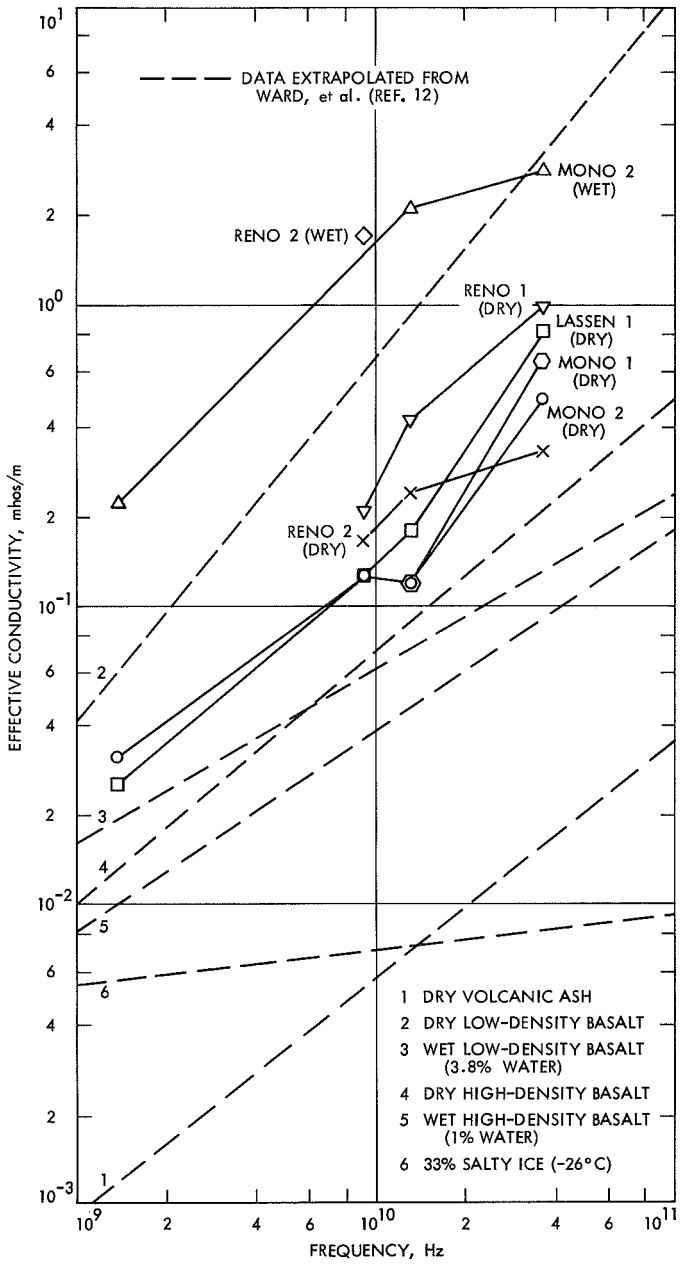

Fig. 8. Comparison of σ_e with extrapolated experimental data

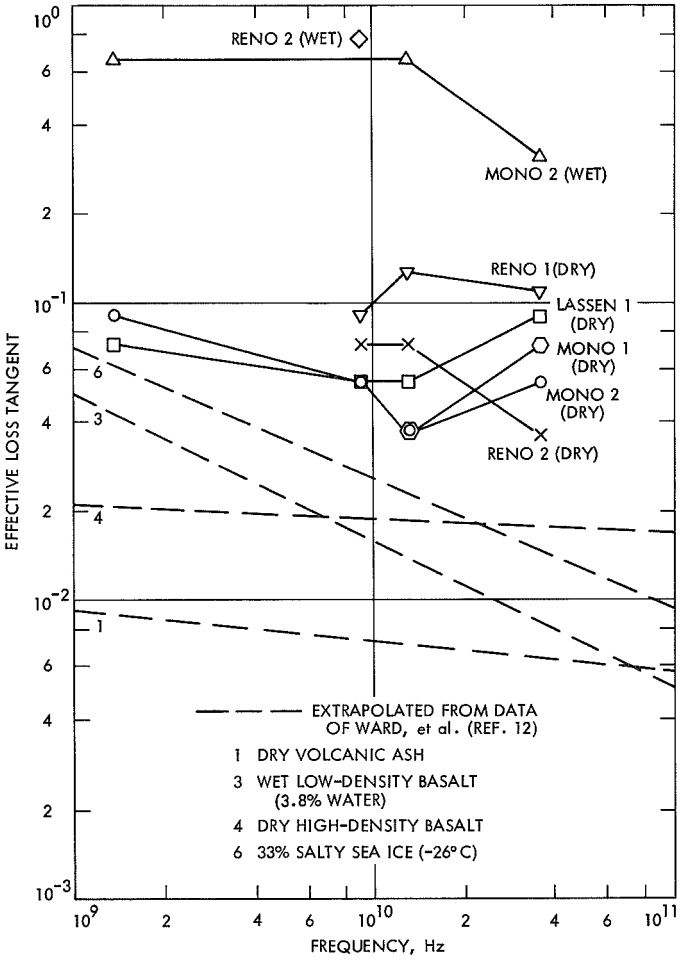

Fig. 9. Comparison of tan δ_e with extrapolated experimental data

complex refractive index in terms of single particle scattering properties, as has been done. A partial physical explanation of this circumstance* may be that in a loose granular aggregate containing moisture predominantly on grain surfaces, pore spaces act as scattering volumes rather than individual grains. Thus, the separation between scatterers is of the order of the grain size. The condition that mutual particle distances be $\gg \lambda$ is partially satisfied, but obviously breaks down when particle size is on the order of λ or larger. Therefore, other physically plausible explanations of the seeming correspondence are required.

IV. Effects of Scattering

The effects of scattering are analyzed by utilizing solutions of the equation of radiative transfer obtained with the so-called two beam approximation. Details of the derivations and notation used are given in the Appendix. A plane-parallel layer of normal thickness l is assumed bounded on one side by a reflecting substrate with reflectance ρ. The radiative properties of the layer are now characterized by mass absorption and scattering coefficients k and s, which may be functions of frequency and position.

If the radiating media are at the same constant temperature, the parameter of previous analysis is replaced by

$$\psi_1(\tau_1) = 1 - \left\{\frac{E(\tau_1)}{E(\infty)}\left[1 + \rho\mathbf{T}(\tau_1)\mathbf{S}(\tau_1)\right] + (1-\rho)\frac{B(T_p)}{E(\infty)}\,\mathbf{T}(\tau_1)\,\mathbf{S}(\tau_1)\right\} \tag{15}$$

where

$$\mathbf{S}(\tau_1) = \frac{1}{[1 - \rho\mathbf{R}(\tau_1)]} \tag{16}$$

The remaining functions in Eq. (15) have been defined in the Appendix. The function $\psi_1(\tau_1)$ is plotted in Fig. 10 for various values of plate reflectance and s/k, the ratio of scattering to absorption coefficients. In general, one expects

$$\left[\frac{I(0)_{\tau_1}}{I(0)_\infty}\right]_{s+a} < \left[\frac{I(0)_{\tau_1}}{I(0)_\infty}\right]_a$$

where $s + a$ means scattering and absorption. Since for an infinitely thick isothermal layer

$$[I(0)_\infty]_{s+a} = \frac{2\xi}{1+\xi}\,[I(0)_\infty]_a$$

one finds

$$[I(0)_{\tau_1}]_{s+a} < \frac{2\xi}{1+\xi}\,[I(0)_{\tau_1}]_a$$

where $\xi = 1/(1 + s/k)$.

Thus, the mean intensity of radiation from a layer of optical thickness τ_1 is less than the mean intensity from a purely absorbing layer of the same thickness by a factor of at least $2\xi/(1+\xi)$, which is the emissivity of a medium of infinite optical thickness expressed in terms of the absorption and scattering coefficients (see Appendix). From Fig. 10, the situation for a perfectly reflecting (nonemitting) substrate conforms to our expectation that the emergent intensity decreases as the ratio s/k increases. For a partially reflecting substrate, the situation is complicated. In terms of the variables plotted, the parameter $\psi_1(\tau_1)$ increases as s/k decreases, and $\psi_1(0)$ decreases as this ratio increases. These complications result because the total emergent intensity (involving both layer and substrate components) has been normalized to the intensity from a medium of infinite thickness (see Appendix Eq. A-11). Thus, from Eq. (15), $\psi_1(0) = 1 - (1-\rho)\,B(T_p)/E(\infty)$.

It should be noted also that with a perfectly reflecting substrate (the situation of principal concern here), the effect on $\psi(\tau_1)$ of a scattering coefficient five times the value of the absorption coefficient is small in terms of the variables used. For $s/k > 5$, the changes in $\psi(\tau_1)$ are on the order of 10^{-3} or smaller.

In nature, one might expect stratified systems involving a poorly conducting layer overlying a substrate of good

*This possibility was called to my attention by Dr. R. J. Phillips.

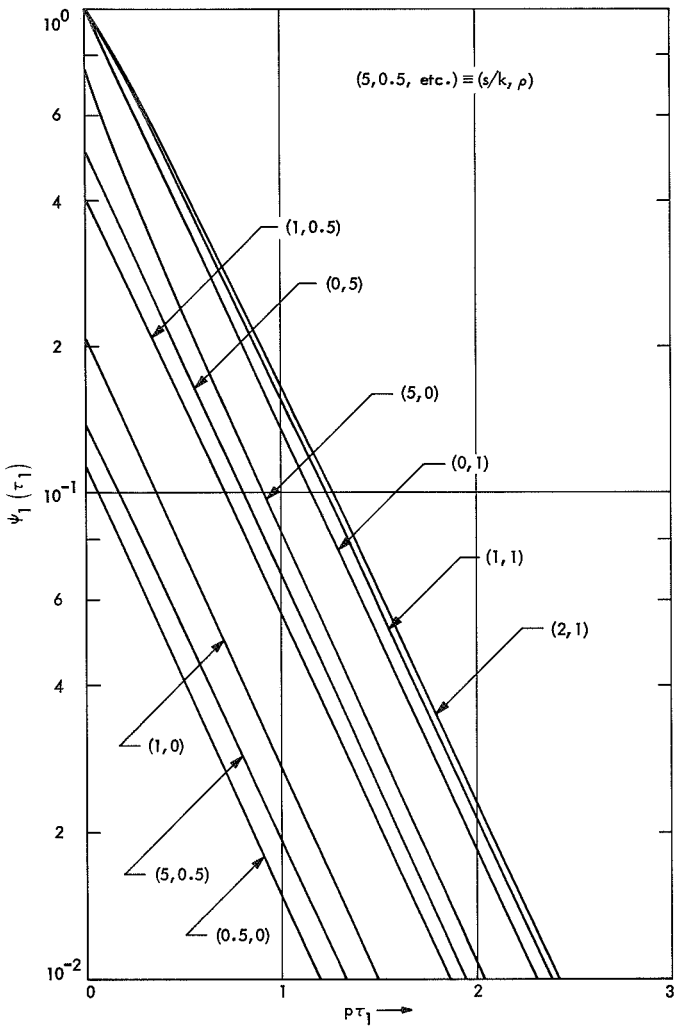

Fig. 10. Effects of scattering on ψ

conductor to be associated with ground water or permafrost. Detection of such nonhomogeneities in otherwise thermally uniform ground might be possible if the reflecting layer varied in depth from one place to another. In such cases, the experimentally determined parameter $\psi(\tau_1)$ would not, when extrapolated to zero layer thickness, pass through the origin. Extraction of layer thickness, or scattering properties from such data would seem to be difficult, however. From the previous discussion, this method appears applicable for determination of layering only if such nonhomogeneities occur within a wavelength or so of the surface in rocks with moisture contents similar to those dealt with here.

V. Summary of Results

A simple radiative transfer theory, neglecting scattering, leads to a qualitative description of passive microwave emission from plane-layered media. The monochromatic microwave absorption coefficient can be determined from such measurements.

The fundamental experimental finding of this study is that k, the mass absorption coefficient, is frequency-independent over the range of frequencies involved (10^9–10^{10} Hz). Effective electrical conductivities are calculated from the data for reasonable values of the dielectric constant in this frequency range. Conductivities obtained are largely dependent on moisture content and generally increase with frequency; they are in approximate agreement with extrapolated results from laboratory experiments, thus substantiating the approximations employed.

Scattering acts to decrease the flow of radiation from the medium, as one expects intuitively. Calculated attenuation lengths vary between 0.05 m (at $\lambda = 1.4$ cm) and 0.5 m ($\lambda = 21$ cm) in materials studied and are strong functions of moisture content. Greater depths could be expected in completely dry material. These depths correspond roughly to "sounding" depths for planetary radar experiments at these wavelengths in such materials.

Appendix

Derivation of Equations Describing Effects of Scattering

Derivation of Eqs. (15) and (16), describing effects of scattering in the radiative transfer problem dealt with here, proceeds according to the same physical arguments used to obtain Eq. (2). Following Ref. 13, for a homogeneous medium, the mean outward and mean inward intensities—inward in this case means toward the reflecting surface (Fig. A-1)—are:

$$2I(\tau) = (1 - \xi)Pe^{-p\tau} + (1 + \xi)Q\,e^{p\tau} + g(\tau) \qquad \text{(A-1)}$$

$$2I'(\tau) = (1 + \xi)Pe^{-p\tau} + (1 - \xi)Q\,e^{p\tau} + h(\tau) \qquad \text{(A-2)}$$

$$I(\tau) = \frac{1}{2\pi}\int_{\text{out}} I(\tau,\theta)d\Omega \qquad \text{(A-3)}$$

$$I'(\tau) = \frac{1}{2\pi}\int_{\text{in}} I(\tau,\theta)d\Omega \qquad \text{(A-4)}$$

where, in Eqs. (A-3) and (A-4), "out" and "in" refer to integrations over solid angle $d\Omega$ in outward and inward hemispheres, and P and Q are arbitrary constants to be satisfied by the boundary conditions. The functions g and h are

$$g(\tau) = (1 + \xi)\int_{\tau}^{\tau_1} B(pt)\,e^{p(\tau-t)}\,d(pt) + (1 - \xi)\int_{0}^{\tau} B(pt)\,e^{-p(\tau-t)}\,d(pt) \qquad \text{(A-5)}$$

$$h(\tau) = (1 - \xi)\int_{\tau}^{\tau_1} B(pt)\,e^{p(\tau-t)}\,d(pt) + (1 + \xi)\int_{0}^{\tau} B(pt)\,e^{-p(\tau-t)}\,d(pt) \qquad \text{(A-6)}$$

in which $B(t)$ is the Planck function,

$$p = \kappa\xi$$

$$\kappa = \frac{(k + s)}{(\bar{k} + \bar{s})}$$

$$\xi = \frac{1}{\left(1 + \dfrac{s}{k}\right)}$$

$$d\tau = 2(\bar{k} + \bar{s})\delta\,dx$$

In these expressions, $\bar{k}$ and $\bar{s}$ are mean values of the absorption and scattering coefficients averaged through the spectrum, and δ is density.

The ultimate goal is to find the intensity emergent from a layer of optical thickness τ_1 with a second, perhaps partially reflecting medium, below τ_1. The emergent radiation at $\tau = 0$ is composed of the following:

(1) Intensity emitted directly in outward direction by the medium.

(2) Intensity emitted by the reflecting substrate after attenuation by the layer.

(3) Intensity emitted in inward direction after reflection by the substrate and attenuation by the layer.

(4) Intensity of light multiply reflected by the medium and substrate and attenuated by the layer.

The reflection and transmission coefficients for an absorbing, scattering layer of optical thickness τ are derived from Eqs. (A-1) and (A-2) with $g(\tau) = h(\tau) = 0$ under the following boundary conditions:

$$I'(0) = \text{const at } \tau = 0$$

$$I(\tau_1) = 0 \text{ at } \tau = \tau_1$$

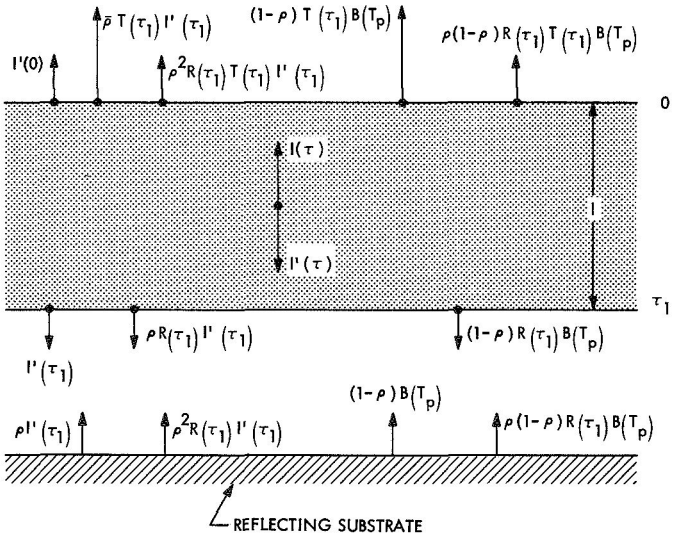

Fig. A-1. Emission from layer with reflecting substrate, including multiple reflections

These coefficients for a layer of optical thickness τ_1 are

$$\mathbf{R}(\tau_1) = I(0)/\text{const} = \frac{2R \sinh p\tau_1}{\Delta(\tau_1)} \tag{A-7}$$

and

$$\mathbf{T}(\tau_1) = I'(\tau_1)/\text{const} = \frac{(1 - R^2)}{\Delta(\tau_1)} \tag{A-8}$$

in which

$$R = \frac{(1 - \xi)}{(1 + \xi)}$$

and

$$\Delta(\tau_1) = e^{p\tau_1} - R^2 e^{-p\tau_1}$$

The intensity of light emitted by a layer (considered for the moment without reflecting substrate) depends upon whether we consider inward or outward directed beams. This component of this intensity is derived from Eqs. (A-1) and (A-2) with the boundary conditions

$$I'(0) = 0 \qquad \text{at } \tau = 0$$
$$I(\tau_1) = 0 \qquad \text{at } \tau = \tau_1$$

and in the general case with $g(\tau)$, $h(\tau) \neq 0$. Thus, computing the emergent intensity at τ_1, for an unconfined nonisothermal layer, one obtains

$$I'(\tau_1) = \left(\frac{1 + \xi}{2}\right)\left\{\chi(\tau_1) - \frac{R}{\Delta(\tau_1)}\left[(1 - R^2)\,\phi(\tau_1) + 2R \sinh p\tau_1\,\chi(\tau_1)\right]\right\} \tag{A-9}$$

while at $\tau = 0$,

$$I(0) = \left(\frac{1 + \xi}{2}\right)\left\{\phi(\tau_1) - \frac{R}{\Delta(\tau_1)}\left[(1 - R^2)\,\chi(\tau_1) + 2R \sinh p\tau_1\,\phi(\tau_1)\right]\right\} \tag{A-10}$$

in which

$$\phi(\tau_1) = \int_0^{\tau_1} B(pt)\, e^{-pt}\, d(pt)$$

$$\chi(\tau_1) = \int_0^{\tau_1} B(pt)\, e^{-p(\tau_1 - t)}\, d(pt)$$

If B = constant, $\phi = \chi = B(1 - e^{-p\tau_1})$. Thus from either Eq. (A-9) or Eq. (A-10) one finds

$$\lim_{\tau_1 \to \infty} [E(\tau_1), E'(\tau_1)] = \frac{2\xi}{1 + \xi} B(T) \tag{A-11}$$

where T is the absolute temperature, and substitutions have been made

$$E(\tau_1) = I(0)$$
$$E'(\tau_1) = I'(\tau_1)$$

The factor involving ξ in Eq. (A-11) is the emittance of a medium of infinite optical thickness, and the parameter R is the reflectance.

Equations (A-9) and (A-10) show that, for a nonisothermal medium, the emergent intensity depends upon the direction in which the intensity is measured. This is physically reasonable. The anisotropy is illustrated by a simple example. Suppose temperature increases with optical depth; then deeper, hotter layers contribute less to the intensity $I(0)$ than to $I'(\tau_1)$. For isothermal conditions or where $B(t)$ is symmetric about the median plane, this situation does not apply, and the intensity is exactly the same from either side of the layer.

Using Eqs. (A-7) through (A-10), an expression for the emergent intensity $I(0)$ is derived as shown in the following. Referring to Fig. A-1, one finds the contributing terms to I_{out} to be

$$\begin{aligned} I_{\text{out}} = {} & E(\tau_1) + \rho\mathbf{T}(\tau_1)E'(\tau_1) \\ & + \rho\mathbf{R}(\tau_1)\mathbf{T}(\tau_1)\,[\rho E'(\tau_1)] \\ & + \rho\mathbf{R}(\tau_1)\mathbf{T}(\tau_1)\{\rho\mathbf{R}(\tau_1)\,[\rho E'(\tau_1)]\} \\ & + \cdots \\ & + (1 - \rho)\mathbf{T}(\tau_1)B(T_p) \\ & + \rho\mathbf{R}(\tau_1)\mathbf{T}(\tau_1)\;[(1 - \rho)B(T_p)] \\ & + \rho\mathbf{R}(\tau_1)\mathbf{T}(\tau_1)\,\{\rho\mathbf{R}(\tau_1)\,[(1 - \rho)B(T_p)]\} \\ & + \cdots \end{aligned}$$

or rearranging

$$I_{\text{out}} = E(\tau_1) + \rho\mathbf{T}(\tau_1)E'(\tau_1) \times [1 + \rho\mathbf{R}(\tau_1) + \overline{\rho\mathbf{R}(\tau_1)}^2 + \cdots] + (1-\rho)\mathbf{T}(\tau_1)B(T_p) \times [1 + \rho\mathbf{R}(\tau_1) + \overline{\rho\mathbf{R}(\tau_1)}^2 + \cdots]$$

Using the progression

$$\sum_{k=0}^{\infty} q^k = \frac{1}{1-q} \qquad [|q| < 1]$$

this result may be written

$$I_{\text{out}} = E(\tau_1) + \frac{\rho\mathbf{T}(\tau_1)E'(\tau_1)}{[1-\rho\mathbf{R}(\tau_1)]} + \frac{(1-\rho)\mathbf{T}(\tau_1)B(T_p)}{[1-\rho\mathbf{R}(\tau_1)]} \tag{A-12}$$

For large τ_1, $I_{\text{out}} \to E(\tau_1)$, and

$$\lim_{\tau_1 \to \infty} E(\tau_1) = \frac{2\xi}{1+\xi}\int_0^{\infty} B(pt)\, e^{-pt}\, d(pt)$$

Text Eq. (15) follows from Eqs. (A-11) and (A-12), and the definition of ψ.

If $s \to 0$, corresponding to a purely absorbing medium, $\xi \to 1$, and $R \to 0$. Thus, from Eqs. (A-7), (A-8), and (A-12), with B constant,

$$\lim_{\xi \to 1} \begin{cases} \mathbf{R}(\tau_1) \to 0 & \text{(A-13)} \\ \mathbf{T}(\tau_1) \to e^{-p\tau_1} & \text{(A-14)} \\ E(\tau_1) = E'(\tau_1) \to B(1 - e^{-p\tau_1}) & \text{(A-15)} \end{cases}$$

and

$$I_{\text{out}} = B(1 - e^{-p\tau_1}) + \rho\, e^{-p\tau_1} B(1 - e^{-p\tau_1}) + (1-\rho)\, e^{-p\tau_1} B(T_p) \tag{A-16}$$

in agreement with text Eq. (2).

Nonhomogeneous media will often be encountered when dealing with natural surfaces, as already pointed out in the text. One way of treating plane-layered solids is by ray-tracing, which proceeds as outlined in the following. We imagine the nonhomogeneous medium to be stratified parallel to the outer boundary or surface, and consider individual layers to be homogeneous, but, in general, nonisothermal. Consider a pair of layers, the nth and $(n+1)$th. From Fig. A-2, one can compute the outward intensity from the nth layer I_n, which results from radiation from each layer, and from externally incident radiation. For layers inside the medium, intensities I'_n, I_{n+1} are contributions from succeeding layers above and below the pair $(n, n+1)$. Taking account of multiple reflections in the manner indicated in the figure, one arrives at expressions for the intensities I_n and I'_{n+1} in the form

$$I_n = E_n + E_{n+1}\mathbf{T}_n(1 + \mathbf{R}_n\mathbf{R}_{n+1}\mathbf{S}_{n,\,n+1}) + E'_n\mathbf{R}_{n+1}\mathbf{T}_n\mathbf{S}_{n,\,n+1} + I'_n(\mathbf{R}_n + \mathbf{R}_{n+1}\mathbf{T}_n^2\mathbf{S}_{n,\,n+1}) + I_{n+1}\mathbf{T}_n\mathbf{T}_{n+1}\mathbf{S}_{n,\,n+1} \tag{A-17}$$

$$I'_{n+1} = E'_{n+1} + E'_n\mathbf{T}_{n+1}(1 + \mathbf{R}_{n+1}\mathbf{R}_n\mathbf{S}_{n+1,\,n}) + E_{n+1}\mathbf{R}_n\mathbf{T}_{n+1}\mathbf{S}_{n+1,\,n} + I_{n+1}(\mathbf{R}_{n+1} + \mathbf{R}_n\mathbf{T}_{n+1}^2\mathbf{S}_{n+1,\,n}) + I'_n\mathbf{T}_{n+1}\mathbf{T}_n\mathbf{S}_{n+1,\,n} \tag{A-18}$$

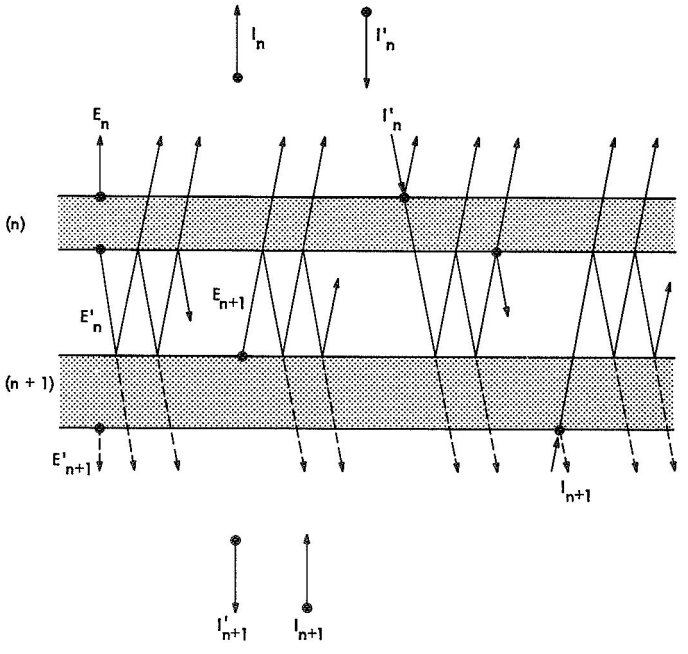

Fig. A-2. Ray paths used in calculating emergent intensities from a two-layer nonhomogeneous medium

where

$$\mathbf{S}_{n,\,n+1} = \mathbf{S}_{n+1,\,n} = \sum_{k=0}^{\infty} (\mathbf{R}_n \mathbf{R}_{n+1})^k$$

$$= \frac{1}{1 - \mathbf{R}_n \mathbf{R}_{n+1}}$$

and $\mathbf{R}_n$ and $\mathbf{T}_n$ are reflection and transmission coefficients of the nth layer defined in analogy with Eqs. (A-7) and (A-8).

To compute the intensity emergent from a medium consisting of M layers, one needs to specify the inward intensity at the surface I'_1, and the outward intensity at the bottom, I_M. Starting at the surface, it may be seen from Eq. (A-17) that the expression for I_1 involves terms in I'_1 and I_2, and that I_2 is a function of I'_2 and I_3, the former being given by Eq. (A-18). Continuing in this fashion, one can carry the calculation through the medium to include all the layers. Clearly, the resulting equations are complicated even considering only a few layers. To illustrate these results, write out the expression for I_1 with $M = 2$ and with $I'_1 = I_2 = 0$. Thus,

$$I_1 = E_1 + E'_1 \mathbf{R}_2 \mathbf{T}_1 \mathbf{S}_{1,2} + E_2 \mathbf{T}_1 \mathbf{S}_{1,2} \qquad \text{(A-19)}$$

where we have used the relation

$$\mathbf{S}_{1,2} = 1 + \mathbf{R}_1 \mathbf{R}_2 \mathbf{S}_{1,2}$$

Eq. (A-19) is equivalent to Eq. (A-12) with

$$\rho = \mathbf{R}_2$$

and

$$(1 - \rho)B(T_p) = E_2$$

From the theory of heat conduction, the temperature distribution throughout the medium is governed by: (1) appropriate boundary conditions, (2) temperatures in two adjoining layers that are equal at an interface, and (3) the net heat flux that remains constant from layer to layer. Thus, in general, E_n and E'_n in each layer can be determined.

References

1. Quade, J. G., Blinn, J. C., Brennin, P. A., and Chapman, P. E., *Multispectral Remote Sensing of an Exposed Volcanic Province,* Technical Memorandum 33-453. Jet Propulsion Laboratory, Pasadena, Calif., June 19, 1970.
2. Sakamoto, S., *Microwave Radiometric Measurements and Ground Truth Investigations,* Report CC-483908. Aerojet-General Corp. Space Division, El Monte, Calif., Aug. 1968.
3. Brennin, P. A., Chapman, P. E., and Quade, J. G., *JPL Microwave Experiment Support,* Technical Letter 15. Mackay School of Mines, University of Nevada, Reno, Nev., Nov. 1968.
4. Piddington, J. H., and Minnett, H. C., "Microwave Thermal Radiation From the Moon," *Austral. J. Sci. Res., Ser. A.,* Vol. 2, No. 63, 1949.
5. Baldwin, J. E., "Thermal Radiation From the Moon and Heat Flow Through the Lunar Surface," *Mon. Not. Roy. Astron. Soc.,* Vol. 122, pp. 513–522, 1961.
6. Hagfors, T., "Remote Probing of the Moon by Infrared and Microwave Emissions and by Radar," *Rad. Sci.,* Vol. 5, No. 2, pp. 189–227, Feb. 1970.
7. Chanine, M. T., "Determination of the Temperature Profile in an Atmosphere From Its Outgoing Radiance," *J. Opt. Soc. Am.,* Vol. 58, No. 12, pp. 1634–1637, 1968.
8. Ward, S. H., *Electromagnetic Exploration of the Moon,* Contract Document NAS2-4720 (preliminary report to be released as NASA special publication). National Aeronautics and Space Administration, Washington.
9. Van de Hulst, H. C., *Light Scattering by Small Particles.* John Wiley & Sons, Inc., New York, 1957.
10. Born, M., and Wolf, E., *Principles of Optics,* Second Edition. The Macmillan Company, New York, 1964.
11. Stratton, J. A., *Electromagnetic Theory.* McGraw-Hill Book Co., Inc., New York, 1941.
12. Ward, S. H., Jiracek, G. R., and Linlor, W. I., "Electromagnetic Reflection From a Plane Layered Lunar Model," *J. Geophys. Res.,* Vol. 73, No. 4, pp. 1355–1372, Feb. 15, 1968.
13. Milne, E. A., "Thermodynamics of the Stars," *Handb. d. Astrophys.,* Vol. 3, Part I, 1930.

NASA — JPL — Coml., L.A., Calif.